Compositional Fragmentation Model for the Oxidation of Sulfide Particles in a Flash Reactor

VÍCTOR ROBERTO PARRA-SÁNCHEZ, MANUEL PÉREZ-TELLO, CIRILO ANDRÉS DUARTE-RUIZ, and HONG YONG SOHN

A mathematical model to predict the size distribution and chemical composition of a cloud of sulfide particles during high-temperature oxidation in a flash reactor is presented. The model incorporates the expansion and further fragmentation of the reacting particles along their trajectories throughout the reaction chamber. A relevant feature of the present formulation is its flexibility to treat a variety of flash reacting systems, such as the flash smelting and flash converting processes. This is accomplished by computing the chemical composition of individual particles and the size distribution and overall composition of the particle cloud in separate modules, which are coupled through a database of particle properties previously stored on disk. The flash converting of solid copper mattes is considered as an example. The model predictions showed good agreement with the experimental data collected in a large laboratory reactor in terms of particle size distribution and sulfur remaining in the population of particles. The cumulative contribution and distribution coefficients are introduced to quantify the relationship between specific particle sizes in the feed and those in the reacted products upon oxidation, the latter of which has practical implications on the amount and chemical composition of dust particles produced during the industrial operation.

DOI: 10.1007/s11663-013-9963-0

I. INTRODUCTION

THE oxidation of sulfide particles at high temperatures in flash smelting and flash converting reactors typically involves significant changes in morphology, size, and chemical composition. Over the last decades, significant experimentation has been conducted[1–16] to elucidate the reaction path followed by the particles during oxidation in the reaction chamber of such furnaces. Although the oxidation reactions occurring in the particles in the two processes are different, the physical changes experienced by the particles show similar characteristics, and they are generally explained in terms of the qualitative model developed by Kim and Themelis[6] and further modified by Jokilaakso *et al.*[8] According to this model, initially nonporous particles that enter the reactor are quickly dispersed and heated up by the process gas and the reactor walls. After ignition, the particles start oxidation and a porous oxide layer is formed surrounding the core of the unreacted sulfides, whereas the gaseous product (sulfur dioxide) is released to the surrounding gas phase. Because the oxidation reactions are highly exothermic, particle temperature increases rapidly, and the melting point of the sulfide core is reached. Further oxidation of the partially molten particle produces small bubbles of sulfur dioxide gas. Because the rate of generation of bubbles is higher than the rate of escape of sulfur dioxide gas through the porous oxide crust, the bubbles accumulate and coalesce within the core of molten sulfides, thus building up the internal pressure and pushing the outer layer of metallic oxides. This in turn causes the particle to expand into a larger sphere. When the internal gas pressure exceeds the surface tension on the particle surface, the particle loses integrity and undergoes fragmentation. While this releases the internal gas pressure, it also produces a number of solid fragments and droplets which are expelled to the surrounding gas. The size, number, and chemical composition of the resulting fragments strongly depend on the initial size and chemical composition of the sulfide particles as well as the operating conditions prevailing in the furnace.

The fragmentation of sulfide particles has generally been accepted as a major source of dust in both flash smelting and flash converting furnaces. Dust consists of fine solid or molten particles with typical sizes less than 20 μm. Dust is undesirable because it tends to be carried away by the off-gas stream toward the uptake shaft, waste heat boiler, and electrostatic precipitator, where they cause a number of operational problems. They also represent a potential hazard to the environment because they can escape to the surrounding atmosphere during the converting step. So far, little attention has been paid to the quantitative aspects of particle fragmentation. For instance, measurements of the size distribution of the particle cloud as it travels through the reaction

VÍCTOR ROBERTO PARRA-SÁNCHEZ and CIRILO ANDRÉS DUARTE-RUIZ, Graduate Students, and MANUEL PÉREZ-TELLO, Professor, are with Department of Chemical Engineering and Metallurgy, University of Sonora, Hermosillo, Sonora 83000, Mexico. Contact e-mail: mperezt@iq.uson.mx HONG YONG SOHN, Professor, is with the Department of Metallurgical Engineering, University of Utah, Salt Lake City, UT 84112.
Manuscript submitted April 20, 2013.

Published online: 08 October 2013

chamber are scarce, and so are mathematical models to describe particle fragmentation from a fundamental standpoint. The present work is part of an ongoing research aimed at characterizing the mechanisms governing particle fragmentation during the oxidation of sulfide particles in flash reactors using a quantitative approach. For that purpose, both experimental work and mathematical modeling is being conducted. In a previous paper,[17] the authors reported on the first mathematical model of particle fragmentation during the flash converting of copper matte particles. The model was constructed in a Lagrangian framework and included five parameters, all of them with physical significance. As a first approximation, the model did not incorporate the oxidation reactions, and thus the mass of individual particles was assumed to be constant during flight. The particle size distribution predicted by the model was compared with the experimental data collected in a laboratory flash converting furnace at the University of Utah.[18] Overall, good agreement between the predicted and the experimental values was obtained. However, the size fraction corresponding to dust particles (<20 μm) showed the largest discrepancy with the experimental data. This was attributed to the model assumption of constant particle mass, which resulted from neglecting the oxidation reactions.

Whereas an accurate calculation of the amount of dust in the particle population is relevant for both flash smelting and flash converting operations, it is also desirable that the chemical composition of the particle cloud may be computed, so that a complete characterization of the particle population within the reactor can be made. In this paper, a mathematical formulation capable of achieving both tasks is referred to as compositional fragmentation model (CFM). The goal of this investigation was twofold: (1) to develop a CFM capable of improving the model predictions previously obtained for flash converting of solid copper mattes,[17] and (2) to develop a flexible formulation capable of extending the mathematical treatment to other processes such as flash smelting of copper concentrates.

II. MODEL FORMULATION

Figure 1 shows a schematic representation of the present model, which is set up in a Lagrangian framework. Thus, the trajectory of individual particles is tracked as they travel through the reaction chamber. Particles are assumed to be spherical and initially nonporous. They are also assumed to travel at a constant velocity. As was previously discussed by the authors,[17] these assumptions agree with the experimental observations[18] and with computational fluid dynamic calculations of the laboratory flash converting furnace at the University of Utah.[19] In a more general context, they are also valid for most experimental studies on the oxidation of sulfide particles in laminar-flow reactors reported in the literature.[1–14] In flash smelting and flash converting furnaces, the fraction of the reaction chamber occupied by the particles is less than 0.1 pct by volume. Under such conditions, the collision and further agglomeration of particles during flight is unlikely because the particle suspension is dilute. Although some agglomerates were observed experimentally,[18] they are likely to be formed during sampling before the particles quenched. Therefore, the present model does not consider agglomeration of particles during flight. Other assumptions made in the present formulation are described later.

Figure 1 shows the oxidation of copper matte particles during flash converting, which is considered here as an example. As will be clarified later in this paper, this is not a limitation of the present formulation. By writing the appropriate kinetic model, other oxidation reactions can be readily adapted without change of the mathematical framework described below.

The starting point is a copper matte particle with size x_{i0} which enters the reaction chamber. Once the particle gets ignited, the oxidation reactions will cause the particle to expand at a constant rate g, so that its size x_i at time t will be

$$x_i = x_{i0} + gt \quad i = 1, n \qquad [1]$$

where subscript i indicates the ith size fraction in the feed, and n is the total number of size fractions in the feed. The particle expansion rate g was assumed to be independent of particle size. During the flight, the particle expands until it reaches a critical size x_{ic} which is dependent upon its initial size:

$$x_{ic} = f_c x_{i0} \quad i = 1, n \qquad [2]$$

where f_c is a proportionality constant. Because particles of the same size fraction may follow different trajectories under turbulent conditions, a fraction f_{if} of the population of particles with initial size x_{i0} was assumed to achieve fragmentation upon leaving the reaction chamber. For a fully laminar-flow reactor, it is expected that f_{if} takes on the value of either zero or unity. This is because all the particles with initial size x_{i0} follow identical trajectories in the reactor. The fraction $(1 - f_{if})$ represents the particles that continue expansion in the reaction chamber until they leave the reactor. At the end of the reaction chamber, the oxidation reactions and all physical changes experienced by the particles are assumed to interrupt instantly.

The time spent by the particles to reach their critical size x_{ic} is denoted by t_{ic} and can be computed from Eq. [1] by setting: $x_i = x_{ic}$. Let f_i be the fraction of particles of initial size x_{i0} that fragmented up to time t. Fragmentation was assumed to occur gradually along the particle trajectory according to the following expression:

$$f_i = \frac{(t - t_{ic})}{(t_R - t_{ic})} f_{if} \quad i = 1, n \qquad [3]$$

where $t_R = L/v$ is the mean residence time of the particles, L is the reactor length, and v is the particle velocity, which in the present case was assumed to be constant and equal to 2.3 m/s. Equation [3] satisfies the conditions: $f_i = 0$ for $t = t_{ic}$, and $f = f_{if}$ for $t = t_R$. The fraction of particles that fragmented by the time they reached the exit f_{if} was assumed to be

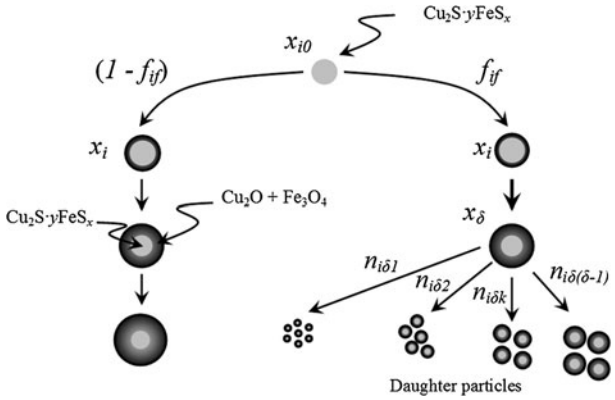

Fig. 1—Schematic representation of the CFM for flash converting of solid copper mattes.

dependent upon the initial particle size according to the functional expression:

$$f_{if} = f_{if}(x_{i0}, f_{2f}, f_{nf}) \quad i = 1, n \qquad [4]$$

where symbols f_{2f} and f_{nf} are adjustable parameters for the initial sizes x_{20} and x_{n0}, which represent the second smallest and the largest size in the feed, respectively. Equation [4] is a general expression for a family of mathematical relationships which are detailed in Appendix. Fragmentation was assumed to produce daughter particles with the same apparent density as their mother particle, *i.e.*,

$$\rho_{i\delta k} = \rho_{i\delta} \quad i = 1, n \quad \delta = i + 1, \tilde{n} \qquad [5]$$

where $\tilde{n}$ is the number of sizes in the population of particles at time t. It is noted that: $\tilde{n} > n$ because particle expansion increases the number of sizes in the population during flight. Equation [5] implies that all the daughter particles are smaller than their mother particle: $x_k < x_\delta$. Once fragmentation occurred, it was further assumed that the daughter particles did not oxidize any further, so that their size and chemical composition remained unchanged throughout the reaction chamber. This assumption was made for mathematical simplicity and may be relaxed in the future as further experimental evidence reveals the reaction path of daughter particles.

Let $n^0_{i\delta k}$ be the number of particles with size x_k which were produced by the fragmentation of a single particle with size x_δ which resulted from the oxidation and expansion of a single particle with initial size x_{i0}. The number of daughter particles produced by the fragmentation of this single particle is denoted by $n^0_{i\delta}$ and is given by

$$n^0_{i\delta} = \sum_{k=1}^{\delta-1} n^0_{i\delta k} \quad i = 1, n \quad \delta = i + 1, \tilde{n} \qquad [6]$$

The fraction of $n^0_{i\delta}$ which corresponds to daughter particles with size x_k is denoted by $\lambda_{i\delta k}$ and is defined by

$$\lambda_{i\delta k} = n^0_{i\delta k} / n^0_{i\delta} \quad i = 1, n \quad \delta = i + 1, \tilde{n} \quad k = 1, \delta - 1 \qquad [7]$$

Substitution of Eq. [7] into Eq. [6] yields:

$$\sum_{k=1}^{\delta-1} \lambda_{i\delta k} = 1 \quad i = 1, n \quad \delta = i + 1, \tilde{n} \qquad [8]$$

Symbol $\lambda_{i\delta k}$ represents the mechanisms governing particle fragmentation, and was represented by the following model:

$$\lambda_{i\delta k} = k_i \left(\frac{x_k}{x_\delta}\right)^\gamma \ln\left(\frac{x_\delta}{x_k}\right) \quad i = 1, n \quad \delta = i + 1, \tilde{n} \quad k = 1, \delta - 1 \qquad [9]$$

where k_i is a proportionality constant and γ is a distribution parameter. Equation [9] is similar to the empirical expressions used to compute the selection function in batch comminution,[20] and is a variation of the previous expression developed by Perez-Tello *et al.*[17] Equation [9] was chosen upon testing a number of mathematical expressions and comparing the model predictions with the experimental data.

In Eq. [9], symbol γ represents the distribution of sizes of the daughter particles upon fragmentation. When $\gamma < 0$, the mother particle produces mostly fine daughter particles; when $\gamma = 0$, the daughter particles distribute uniformly into all size fractions in the range: $x_1 \le x_k < x_\delta$; finally, when $\gamma > 0$, the fragmenting particle produces mostly large daughter particles of similar size to x_δ. Because γ was set to be independent of particle size, particles of all sizes were assumed to fragment similarly. Upon substituting Eq. [9] into Eq. [8], the following expression is obtained

$$k_i = \frac{1}{\sum_{k=1}^{\delta-1} \left(\frac{x_k}{x_\delta}\right)^\gamma \ln\left(\frac{x_\delta}{x_k}\right)} \quad i = 1, n \quad \delta = i + 1, \tilde{n} \qquad [10]$$

Parameter k_i can be computed from Eq. [10] and it can further be used to compute $\lambda_{i\delta k}$ from Eq. [9]. Upon fragmentation, the mass of the mother particle is distributed throughout the daughter particles. Because the density of the daughter particles is assumed to be the same as the density of their mother particle (Eq. [5]), the mass conservation relationship reduces to the volume-conservation expression.

$$x^3_\delta = \sum_{k=1}^{\delta-1} n^0_{i\delta k} x^3_k \quad i = 1, n \quad \delta = i + 1, \tilde{n} \qquad [11]$$

Substitution of Eq. [7] into Eq. [11] yields, upon rearrangement:

$$n^0_{i\delta} = \frac{x^3_\delta}{\sum_{k=1}^{\delta-1} \lambda_{i\delta k} x^3_k} \quad i = 1, n \quad \delta = i + 1, \tilde{n} \qquad [12]$$

The number of daughter particles with size x_k produced by all the particles with initial size x_{i0} that

achieved fragmentation at time t upon reaching size x_δ is denoted by $n_{i\delta k}$. This quantity is obtained by multiplying the number of daughter particles with size x_k produced by a single particle times the total number of particles with initial size x_{i0} that entered the reactor and fragmented at time t; namely,

$$n_{i\delta k} = n^0_{i\delta k} n_i f_i \quad i = 1, n \;\; \delta = i+1, \tilde{n} \;\; k = 1, \delta - 1 \qquad [13]$$

where n_i is the number of particles with initial size x_{i0} in the feed that entered the reactor. This quantity may be obtained from the size distribution of the feed:

$$n_i = \frac{f_3(x_{i0})(\Delta x_{i0}) m_f}{\rho_0 C_3 x^3_{i0}} \quad i = 1, n \qquad [14]$$

where $f_3(x_{i0})$ is the mass density function of size fraction x_{i0} in the feed, Δx_{i0} is the size interval, m_f is the total mass of all the particles of all sizes being fed to the furnace, ρ_0 is the density of the feed particles, and $C_3 = \pi/6$ is the particle shape factor. Equation [14] represents the total mass of particles of size x_{i0} in the feed divided by the mass of a single particle with size x_{i0}. The mass associated with all the particles $n_{i\delta k}$ obtained from Eq. [13] is thus obtained by multiplying $n_{i\delta k}$ by the mass of an individual particle; *i.e.*,

$$m_{i\delta k} = n_{i\delta k} \rho_{i\delta k} C_3 x^3_k \quad i = 1, n \;\; \delta = i+1, \tilde{n} \;\; k = 1, \delta - 1 \qquad [15]$$

Therefore, the mass of all daughter particles with size x_k that were produced at time t upon fragmentation of all the initial sizes x_{i0} that reached size x_δ prior to fragmentation is given by:

$$m_{\delta k} = \sum_{i=1}^{n} m_{i\delta k} \quad \delta = i+1, \tilde{n} \;\; k = 1, \delta - 1 \qquad [16]$$

Similarly, the mass of particles with size x_k that resulted from the expansion of all the particles with initial size x_{l0}, where $x_{l0} < x_k$ at time t, is given by:

$$m_{lk} = (1 - f_l) n_l \rho_{lk} C_3 x^3_k \quad l = 1, k-1 \;\; k = 2, \tilde{n} \qquad [17]$$

Therefore, the total mass of particles with size x_k at time t is given by the summation of all the Eqs. [16] and [17] and is denoted by m_k:

$$m_k = \sum_{\delta=k+1}^{\tilde{n}} m_{\delta k} + \sum_{l=1}^{k-1} m_{lk} \quad k = 1, \tilde{n} \qquad [18]$$

Finally, the mass density function of all the particles with size x_k at time t is computed from the following expression

$$f_3(x_k) = \frac{m_k}{\left(\sum_{k=1}^{\tilde{n}} m_k\right) \Delta x_k} \quad k = 1, \tilde{n} \qquad [19]$$

in which the summation term represents the mass of the particle population at time t. Equation [19] is the final relationship to compute the size distribution of particles in the reaction chamber. When $t < t_R$, quantity $f_3(x_k)$ represents the size distribution along the reactor length, whereas for $t = t_R$ it represents the size distribution at the exit of the reaction chamber.

A relevant feature of the present formulation is its capability to compute the chemical composition of the particle cloud as it travels through the reaction chamber. A mass balance for species q upon fragmentation of a single particle with size x_δ yields:

$$\rho_{i\delta} C_3 x^3_\delta \omega^q_{i\delta} = \sum_{k=1}^{\delta-1} n^0_{i\delta k} \rho_{i\delta k} C_3 x^3_k \omega^q_{i\delta k} \qquad [20]$$
$$i = 1, n \;\; \delta = i+1, \tilde{n} \;\; q = 1, Q$$

where $\omega^q_{i\delta}$ and $\omega^q_{i\delta k}$ represent the mass fraction of species q in the mother particle with size x_δ and the daughter particle with size x_k, respectively. Equation [20] states that the mass of species q in the mother particle distributes into all its daughter particles upon fragmentation. Symbol q may represent either chemical species or chemical elements as long as the following restriction is satisfied

$$\sum_{q=1}^{Q} \omega^q_{i\delta k} = \sum_{q=1}^{Q} \omega^q_{i\delta} = 1 \quad i = 1, n \;\; \delta = i+1, \tilde{n} \;\; k = 1, \delta - 1 \qquad [21]$$

where Q is the total number of chemical species/elements in the particle. Substitution of Eq. [5] and $C_3 = \pi/6$ into Eq. [20] yields

$$x^3_\delta \omega^q_{i\delta} = \sum_{k=1}^{\delta-1} n^0_{i\delta k} x^3_k \omega^q_{i\delta k} \quad i = 1, n \;\; \delta = i+1, \tilde{n} \;\; q = 1, Q \qquad [22]$$

It is noted that Eq. [22] reduces to Eq. [11] by collecting the summation terms over the total number of species Q on both sides of Eq. [22], and further substituting Eq. [21] into the resulting expression. From a numerical standpoint, Q independent equations in the form of Eq. [22] may be written containing: $Q(\delta - 1)$unknowns; namely, the species compositions: $\omega^q_{i\delta k}$. There are also: $(\delta - 1)$ restrictions in the form of the right-hand side of Eq. [21], for a total of: $Q + \delta - 1$ independent equations. The degrees of freedom (DF) of this set of equations are thus: $\mathrm{DF} = Q(\delta - 1) - (Q + \delta - 1)$, which upon simplification yields

$$\mathrm{DF} = Q(\delta - 2) - \delta + 1 \qquad [23]$$

The DF represent the number of $\omega^q_{i\delta k}$ values that should be specified in advance to solve the set of equations [22]. A quick inspection of Eq. [23] shows the magnitude of the numerical challenge to be faced. For flash converting of solid copper mattes: $Q = 4$ ($Cu_2S{\cdot}yFeSx$, Cu_2O, Fe_3O_4, and SiO_2). Thus, Eq. [23] yields: $DF = 3\delta - 7$. This expression indicates that the DF increase by three in consecutive sizes of fragmenting particles. For instance, the DF for sizes x_5 and x_6 are 8 and 11,

respectively. If the size distribution of the particle population were represented by $\tilde{n} = 100$ size fractions, the DF for the largest particle size undergoing fragmentation are 293. For flash smelting of copper concentrates, the problem is even more difficult because the number of species in the particle may be $Q = 7$ or higher,[12] which significantly increases the value of DF.

The previous discussion points to the need for physical knowledge about the mechanisms governing particle fragmentation. This will permit the specification of DF of Eq. [22] based on experimental evidence. Although this information is not yet available, it is generally accepted that the composition of the daughter particles $\omega^q_{i\delta k}$ is dependent upon the history followed by its mother particle in the reaction chamber, and the size of the daughter particle. In functional notation,

$$\omega^q_{i\delta k} = \omega^q_{i\delta k}(\omega^q_{i\delta}, x_k) \quad i = 1, n \;\; \delta = i+1, \tilde{n} \;\; k = 1, \delta - 1 \;\; q = 1, Q \qquad [24]$$

Equation [24] can be inferred from the qualitative model by Jokilaakso *et al.*,[8] which suggests several ways of fragmentation depending upon the operating conditions in the reactor. For instance, small droplets of molten sulfides can be ejected from the particle core while a large, empty shell of copper and iron oxides is left behind. An alternative mechanism may lead to a violent explosion of the fragmenting particle which produces daughter particles of similar size with varying composition. Because the quantitative representations of such mechanisms are yet to be established, in the present formulation it was assumed that the composition of the daughter particles is the same as that of their mother particle,

$$\omega^q_{i\delta k} = \omega^q_{i\delta} \quad i = 1, n \;\; \delta = i+1, \tilde{n} \;\; k = 1, \delta - 1 \;\; q = 1, Q \qquad [25]$$

This assumption may be relaxed in the future as further research clarifies the mathematical structure of Eq. [24]. Furthermore, the mass of species q present in all the particles with size x_k at time t is denoted by m^q_k and was computed from:

$$m^q_k = \sum_{\delta=k+1}^{\tilde{n}} \omega^q_{i\delta} m_{\delta k} + \sum_{l=1}^{k-1} \omega^q_{lk} m_{lk} \quad k = 1, n \; q = 1, Q \qquad [26]$$

in which the first term on the right-hand side represents the mass of the qth species in all the daughter particles with size x_k. Similarly, the second term on the right-hand side is the mass of the qth species in all the particles that expanded up to size x_k. The chemical composition of size fraction x_k at time t is thus obtained by dividing the total mass of species q within the size fraction by the total mass of the given size

$$\omega^q_k = \frac{m^q_k}{m_k} \quad k = 1, \tilde{n} \;\; q = 1, Q \qquad [27]$$

where m_k and m^q_k are computed from Eqs. [18] and [26], respectively. A relevant characteristic of the particle cloud is its overall composition at a given location in the furnace. This quantity is represented by the symbol $\langle \omega^q \rangle$ and is defined by:

$$\langle \omega^q \rangle = \frac{\sum_{k=1}^{\tilde{n}} m^q_k}{\sum_{k=1}^{\tilde{n}} m_k} \quad q = 1, Q \qquad [28]$$

It is noted that $\langle \omega^q \rangle$ represents the composition that may be obtained experimentally by collecting a representative sample of the particle cloud at a given location in the reaction chamber and further conducting its chemical analysis. A common response variable in flash converting and flash smelting operations is the fraction of sulfur remaining in the population of particles. This quantity was computed from the following expression

$$\langle S_{\text{rem}} \rangle = \frac{\sum_{k=1}^{\tilde{n}} \omega^S_k m^S_k}{\sum_{k=1}^{n} \omega^S_{k,0} m^S_{k,0}} \qquad [29]$$

in which subscripts "0" in the denominator refer to the values in the feed, and superscript "*S*" stands for sulfur.

A. *Numerical Solution and Validation of the Mathematical Model*

Before the numerical strategy is described, a brief discussion on the nature of the model parameters is pertinent. Parameter f_c in Eq. [2] establishes the critical diameter at which an initial particle with size x_{i0} initiates fragmentation during flight. Because the reaction path followed by the particles is strongly dependent on its initial size in the feed, it is likely that parameter f_c be size dependent in reality. By extension, other model parameters such as the expansion rate g in Eq. [1] and the fragmentation parameter γ in Eq. [9] are likely to be size dependent as well. Because the size distribution in the feed consists of several hundreds of initial sizes, the incorporation of size dependency to such parameters would lead to several hundreds of adjustable parameters to be computed. This would make the formulation impractical. Therefore, a decision was made to keep the number of parameters to a minimum provided the model predictions are with reasonable agreement with the experimental data. As a result, the present formulation can be fully solved by specifying the size distribution in the feed $f_3(x_{i0})$ and five model parameters: f_c, g, γ, f_{2f}, and f_{nf}.

Equations [15] and [17] require the particle apparent densities: $\rho_{i\delta}$ and ρ_{lk}, whereas Eq. [26] requires the particle compositions: $\omega^q_{i\delta}$ and ω^q_{lk}. These properties depend on the nature of the oxidation reactions, and thus must be obtained from the kinetic model of the reacting particles. The numerical strategy to solve the present formulation relies on the assumption that daughter particles do not oxidize any further in the reactor and their size and chemical composition remain unchanged throughout the reaction chamber. Based on Eqs. [5] and [25], the properties of all the particles within the particle-gas suspension can be obtained from the properties of all the initial particles during flight. Therefore, a table of particle properties can be computed in advance by

considering all the initial sizes x_{i0} in the feed. The resulting database may be represented by the functional expression

$$\Phi_i = \Phi_i(x_{i0}, t) \quad i = 1, n \qquad [30]$$

where Φ_i is any particle property of the initial size x_{i0} at time t, such as particle size, particle density, and chemical composition. Equation [30] involves the solution of the kinetic model for every individual size x_{i0} in the feed along its trajectory in the reaction chamber. In these calculations, it was assumed that the particles undergo oxidation and expansion, but no fragmentation. The property database may be computed and stored on disk previously to solving the CFM. This is a convenient feature because it allows the solution of the CFM in a straight-forward manner. Also, it provides a great flexibility because the property database can be constructed by a separate module. As a result, the present formulation can be readily extended to other systems such as flash smelting of copper concentrates by writing the appropriate module which may be further interfaced with the CFM.

In this study, the flash converting of solid copper mattes was considered as an example. Based on the kinetic model developed by Perez-Tello *et al.*[19] for uniformly sized copper matte particles, a new version for expanding particles was developed. The model is described in Appendix. The property database: $\Phi_i = \Phi_i(x_{i0}, t)$ was then computed and stored on disk at discrete values of time t for all the initial sizes x_{i0} in the feed. Upon reading this information, the values of the particle properties required by the CFM were obtained by interpolation within the values contained in the database.

The validation of the present model was accomplished by comparing the model predictions with the experimental data collected in a large laboratory furnace at the University of Utah. Details of the experimental work are discussed elsewhere,[17,18] thus only a brief description is provided here. In a typical experiment, matte particles and process gas entered the furnace at a constant rate through a pilot-scale burner located on top of the reaction chamber. The particles were oxidized while flowing downwards with the gas, and were collected in a receptacle located at the bottom of the reaction chamber. The receptacle was externally water-cooled to quench the particles and thus interrupt the oxidation reactions. Additional samples were collected along the centerline of the reaction shaft by means of a water-cooled sampling probe. Input variables tested in the experiments included the particle size of the feed, oxygen concentration in the process gas, and the oxygen-to-matte ratio. Response variables measured in the particles included the chemical composition, mineralogy, and size distribution of the particle population. The validation of the present model was conducted with the experimental data collected with high-grade (72 pct Cu) matte particles, which experienced severe fragmentation with substantial generation of dust.

During the validation runs, the values of the model parameters: g, f_c, γ, f_{2f}, and f_{nf} were determined by the following procedure. First, the experimental size distributions in the feed and the receptacle samples were represented, respectively, by the empirical expressions:

$$f_3(x) = bx^c e^{-ax} \qquad [31]$$

and:

$$g_3(x) = b_1 x^{c_1} e^{-a_1 x} + b_2 x^{c_2} e^{-a_2 x} \qquad [32]$$

Parameters a, b, and c in Eqs. [31] and [32] were reported by Pérez-Tello *et al.*[21] Equation [31] was used to calculate the number of particles in every size fraction in the feed according to Eq. [14]. For every size fraction, its size and chemical composition along its trajectory was computed as described previously. Upon reaching the receptacle, the r^2 correlation parameter was computed by

$$r^2 = 1 - \frac{\sum_{i=1}^{\tilde{n}} [g_3(x_i) - f_3(x_i)]^2}{\sum_{i=1}^{\tilde{n}} \left[g_3(x_i) - \overline{g_3(x_i)} \right]^2} \qquad [33]$$

where $g_3(x_i)$ is the ith experimental value computed from Eq. [32], $f_3(x_i)$ is the ith predicted value from Eq. [19], $g_3(x_i)$ is the mean experimental value, and $\tilde{n}$ is the number of size fractions in the population. In this study, it was set: $n = 250$ and: $\tilde{n} = 350$. The model parameters were varied in consecutive iterations until the r^2 value was as close to unity as possible. The generation of new values of the model parameters for consecutive iterations was accomplished by the multivariable Simplex optimization algorithm.[22] Typically, convergence was achieved within 400 iterations.

The validation of the compositional aspects of the present formulation was conducted by comparing the values of $\langle S_{rem} \rangle$ computed from Eq. [29] with the experimental values measured along the centerline of the flash converting furnace.[18] For that purpose, the tortuosity of the oxide shell surrounding the unreacted core of matte τ was used as an adjustable parameter in the kinetic model described in Appendix. During the calculations, it was noted that parameter τ played no significant role on the evolution of the size distribution computed from Eq. [19]. However, it did show a strong effect on the evolution of the compositional aspects of the particle population described by Eqs. [27] through [29]. This feature allowed the calculation of the model parameters sequentially; *i.e.*, parameters: g, f_c, γ, f_{2f} and f_{nf} were computed first by means of the Simplex optimization algorithm mentioned previously; the tortuosity τ was then computed by means of a single variable optimization technique.

III. DISCUSSION OF RESULTS

Table I shows the values of the model parameters obtained by the procedure described above for all the experimental conditions reported by Pérez-Tello *et al.*[18] The last column in Table I shows the values of the correlation parameter r^2 obtained by Eq. [33]. In all

Table I. Experimental conditions and numerical parameters of the CFM

Run	Size Fraction in the Feed (μm)	Oxygen-to-Matte Ratio (kg O_2/kg matte)	Oxygen Concentration in Process Gas (vol pct)	g (μm/s)	$-\gamma$	f_{2f}	f_{nf}	f_c	τ	r^2
1	<37	0.25	70	57	2.41	0.66	−0.06	1.1	800	0.980
2	<37	0.33	70	18	2.37	0.87	−1.62	1.0	950	0.991
3	<37	0.25	100	55	2.54	0.83	−0.15	1.2	1100	0.960
4	<37	0.33	100	55	2.70	0.80	−0.42	1.3	1000	0.976
5	37 to 74	0.25	70	18	2.27	0.22	1.15	1.1	800	0.979
6	37 to 74	0.33	70	38	2.51	0.60	0.91	1.2	700	0.922
7	37 to 74	0.25	100	19	2.33	0.31	0.81	1.1	1100	0.962
8	37 to 74	0.33	100	40	2.53	0.81	0.51	1.2	1000	0.955
9	74 to 105	0.25	70	6	2.62	0.24	0.63	1.0	550	0.939
10	74 to 105	0.33	70	17	2.56	0.39	1.03	1.1	600	0.921
11	74 to 105	0.25	100	6	2.48	0.03	1.08	1.0	750	0.928
12	74 to 105	0.33	100	26	2.66	0.60	0.70	1.1	775	0.913
13	105 to 149	0.25	70	5	2.76	−0.22	1.27	1.0	400	0.906
14	105 to 149	0.33	70	13	2.62	0.45	0.74	1.0	450	0.945
15	105 to 149	0.25	100	6	2.66	0.17	0.99	1.0	600	0.947
16	105 to 149	0.33	100	12	2.81	0.15	1.12	1.0	700	0.906
17	<149	0.25	70	58	2.36	−0.02	1.45	1.0	600	0.986
18	<149	0.33	70	47	2.75	−0.06	1.75	1.1	600	0.954
19	<149	0.25	100	60	2.73	0.21	0.99	1.2	800	0.928
20	<149	0.33	100	51	2.64	0.43	1.11	1.2	800	0.939

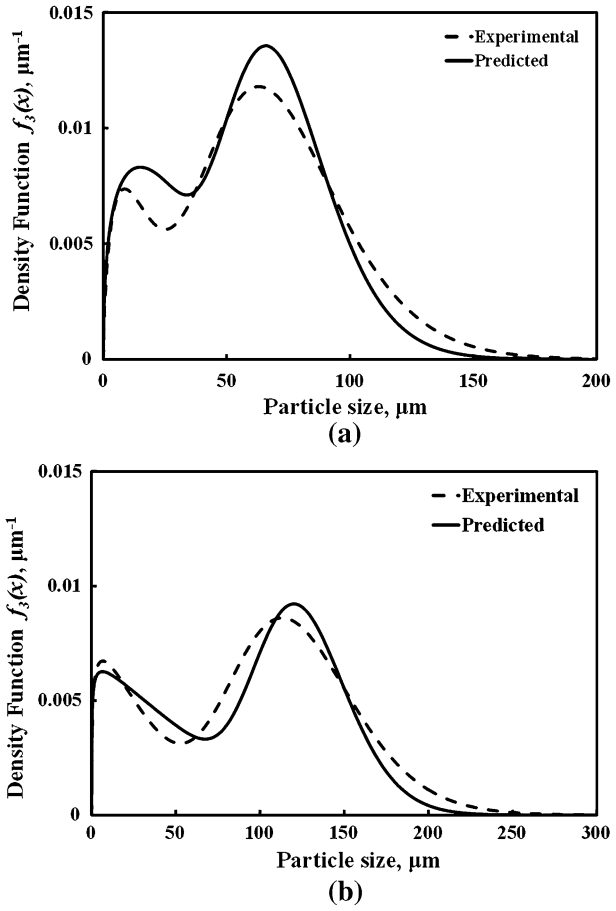

Fig. 2—Experimental and predicted values of the density function in the receptacle of the laboratory flash converting furnace (*a*) run 7, (*b*) run 15.

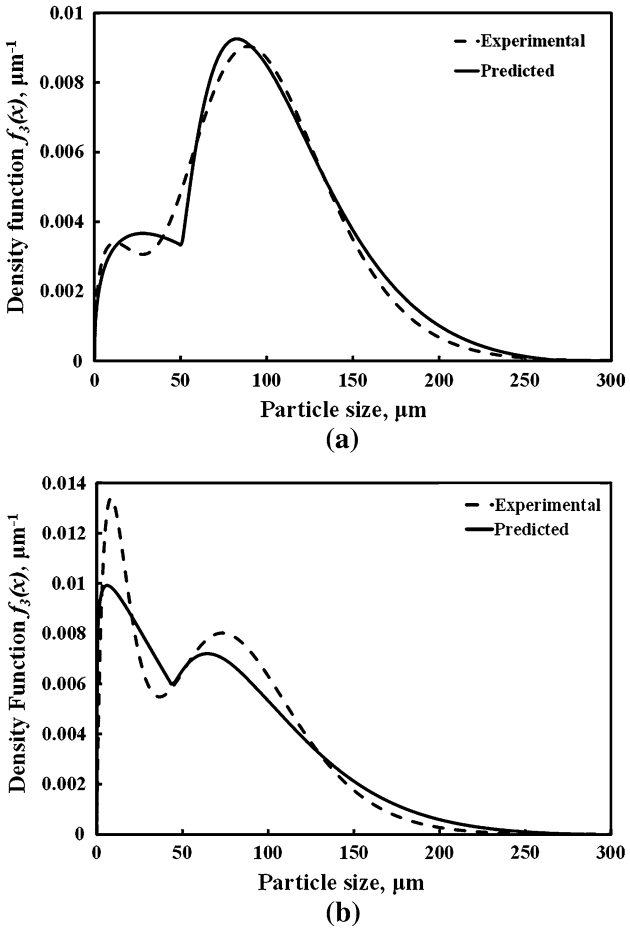

Fig. 3—Experimental and predicted values of the density function in the receptacle of the laboratory flash converting furnace (*a*) run 17, (*b*) run 20.

cases, r^2 is greater than 0.9, thus indicating a good fit with the experimental data regarding particle size distribution. The average value of r^2 in Table I is 0.947, which is larger than the previous value of 0.914 reported by Perez-Tello *et al.*[17] Thus, an overall improvement in the prediction of the particle size distribution was obtained. Examples of the predicted and experimental values of the density functions in the receptacle of the laboratory furnace are shown in Figures 2 and 3. Runs 7 and 15 shown in Figure 2 correspond to the sieved fractions: 37 to 74 and 105 to 149 µm, respectively, whereas runs 17 and 20 shown in Figure 3 correspond to those cases in which the feed to the reactor was not sieved. Overall, a good agreement between the predicted and the experimental values is observed. A relevant feature of the present model is the prediction of the size distribution of dust particles, *i.e.*, those in the range of 0 to 20 µm. From the properties of the density functions, the weight fraction of dust in the particle population may be computed from the following expression:

$$F_{\text{dust}} = \int_0^{20\,\mu\text{m}} f_3(x)dx \qquad [34]$$

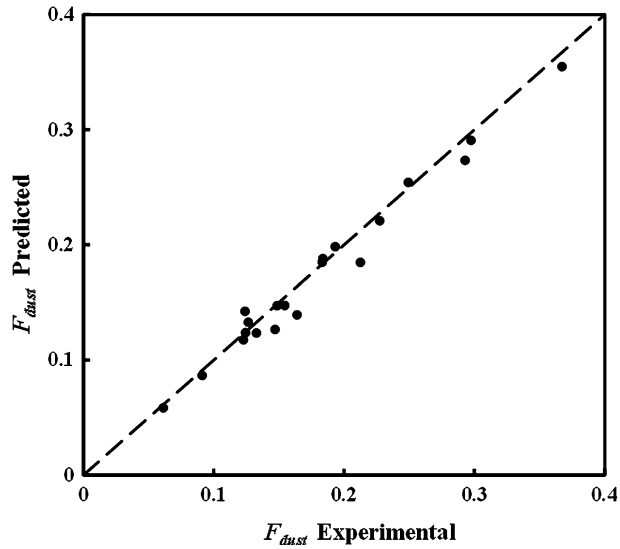

Fig. 4—Predicted and experimental values of the fraction of dust in the receptacle of the flash converting furnace for all the runs shown in Table I.

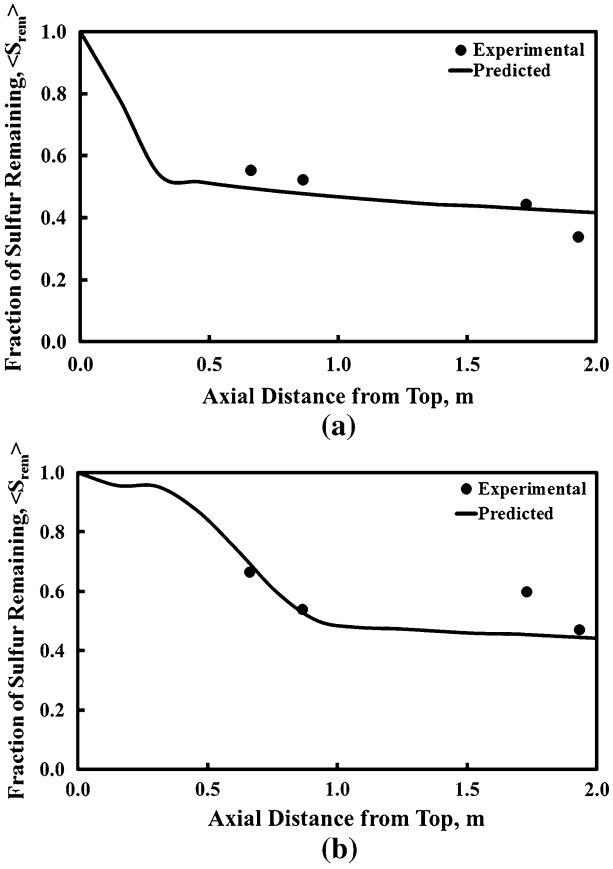

Fig. 5—Predicted and experimental values of sulfur remaining in the population of particles along the flash converting furnace; (*a*) run 7, (*b*) run 15.

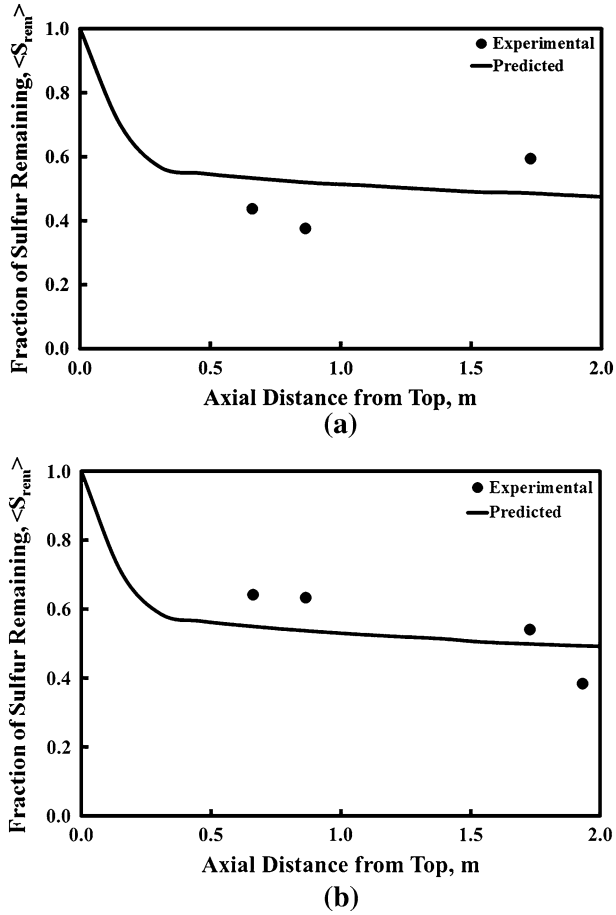

Fig. 6—Predicted and experimental values of sulfur remaining in the population of particles along the flash converting furnace; (*a*) run 17, (*b*) run 20.

Figure 4 shows the computed and the experimental values of F_{dust} for all the experimental conditions shown in Table I. It is noted that most of the points are near the dashed line which represents the perfect agreement between the two values. The maximum error shown in Figure 4 is 15 pct with an average of 6 pct. Thus, a good prediction of the amount of dust in the particle population was obtained.

Figures 5 and 6 show the experimental and computed values of the fraction of sulfur remaining in the population of particles $\langle S_{rem} \rangle$ along the reactor for runs 7, 15, 17, and 20 in Table I, which are shown here as examples. Although the number of experimental data is limited, a good agreement between the predicted and the experimental values is observed. The highest oxidation rate is predicted to occur within the first 0.5 m below the burner tip. The exception is run 15, in which the highest oxidation rate is predicted to occur down to 1 m below the burner tip.

A distinctive feature in Figures 5 and 6 is the shape of the predicted curves, which in all cases show an instantaneous decrease in $\langle S_{rem} \rangle$ as soon as the particle cloud enters the reaction chamber. This behavior is due to the finest particles in the feed, which are rapidly heated up by the reactor walls and ignite shortly after entering the furnace. These particles get fully molten and lose all their sulfur to the gas phase. In contrast, large particles in the feed start reacting farther away in the reactor and do not melt. As a result, once the finest particles in the feed are completely oxidized, the removal of sulfur from the particle cloud occurs gradually along the reactor length. It is common practice to represent the oxidation behavior of a cloud of sulfide particles under suspension-smelting conditions by assuming the feed to be made up of monosize particles, typically the mean size of the feed.[3,12,23] In the present study, it was found that the incorporation of the size distribution in the feed was necessary to represent the experimental data shown in Figures 5 and 6.

Once the mathematical model was validated, it can be used to analyze the main features of a flash converting reactor. The overall capabilities of the expansion-fragmentation model in the absence of oxidation reactions were discussed in the previous paper by Pérez-Tello *et al.*[17] and thus will not be repeated here. In the present paper, emphasis is made on the new capabilities of the improved formulation. The generation of dust is of practical concern in flash smelting and converting operations. In this study, this quantity was defined as follows

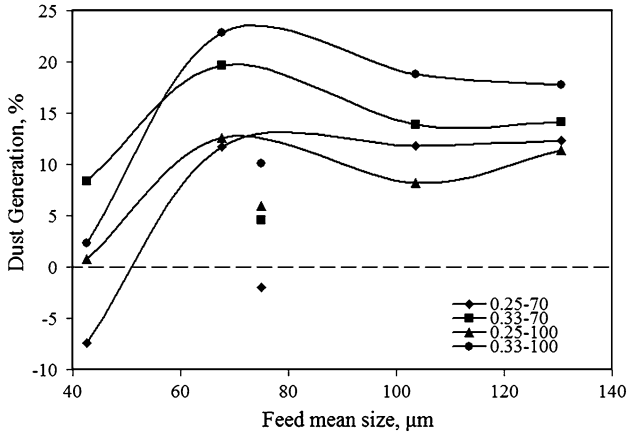

Fig. 7—Dust generation in the laboratory flash converting furnace as a function of the feed mean size, oxygen-to-matte ratio (0.25 and 0.33 kg O_2/kg matte) and oxygen concentration in the process gas (70 and 100 vol pct).

$$\text{Dust Generation (DG)} = \frac{(m_r F_{\text{dust,r}} - m_f F_{\text{dust,f}})}{m_f} \times 100 \quad [35]$$

where m_f and m_r are the mass of the particle population in the feed and the receptacle of the laboratory furnace, respectively. These quantities are equal to the summation term: $\sum_{k=1}^{\tilde{n}} m_k$ computed at times: $t = 0$ and $t = t_R$, respectively. Because of the stoichiometry of the flash converting reaction discussed in Appendix: $m_r < m_f$. The term in parentheses on the right-hand side of Eq. [35] represents the mass of dust generated in the reactor, and is computed as the difference between the mass of dust in the receptacle and that in the feed. Dust generation is then expressed as a weight percentage of the solid feed entering the reactor.

It is noted that DG may be positive, negative or zero depending on the relative amounts of dust in the feed and the receptacle. Positive values of DG indicate that fragmentation prevailed in the furnace, and the amount of dust in the particle population increased upon oxidation. Negative values of DG indicate that particle expansion prevailed in the furnace, and the amount of dust in the particle population decreased upon oxidation. Finally, when DG is zero neither expansion nor fragmentation prevailed, and the amount of dust in the particle population remained unchanged. Because both expansion and fragmentation of particles occur simultaneously in the reaction chamber, the value of DG thus represents the net result of the competition of both phenomena.

Figure 7 shows the values of DG computed from Eq. [35] as a function of the mean size in the feed for all runs shown in Table I. The dashed line represents the hypothetical case: DG = 0 in which no dust is either generated or consumed in the reactor. The isolated symbols correspond to the experiments conducted with the unsieved material (runs 17 through 20), the behavior of which did not follow the trends observed in the sieved fractions of the feed. As expected, most of the experiments produced significant amounts of dust, thus indicating that extensive fragmentation occurred. The value of DG was in the range of 4.5 to 23 pct in 16 out of 20 runs. In contrast, two runs conducted with the size fraction <37 μm produced less than 2.5 pct of dust. The largest positive value of DG was obtained for run 8 in which the sieved fraction: 37 to 74 μm was oxidized under the most severe conditions.

An overall inspection of Figure 7 shows that DG in general increased as the mean size in the feed and the oxygen-to-matte ratio also increased, whereas oxygen concentration in the process gas did not play a significant role on DG. These trends agree with qualitative observations of the reacted particles by scanning electron microscopy[18] which showed that large particles in the feed tended to fragment, whereas small particles in the feed tended to expand upon oxidation. A relevant finding in Figure 7 is the presence of negative values of DG for runs 1 and 17. Therefore, in both runs particle expansion overcame fragmentation, and the amount of dust in the particle population decreased upon oxidation. This suggests the possibility of improving the operation of a flash converting reactor by decreasing the amount of dust that may be carried away by the off-gas stream.

Whereas the value of DG represents the net effect of expansion and fragmentation on the amount of dust in the population of particles, it does not provide further information regarding the origin of dust particles. Let m_{pk} be the mass of size x_k in the population of particles at time t which originated from the initial size in the feed x_{p0}, where: $0 < x_{p0} < x_{i0}$, and let m_k be the mass of all the particles with size x_k. The cumulative contribution of all sizes in the feed within the range: $0 < x_{p0} \leq x_{i0}$ to size x_k in the population is defined by

$$C_{ik} = \sum_{p=1}^{i} \frac{m_{pk}}{m_k} \quad i = 1, n \;\; k = 1, \tilde{n} \quad [36]$$

Symbol C_{ik} is referred to in this paper as the cumulative contribution coefficient from sizes up to x_{i0} in the feed to size x_k in the population of particles. It is noted that C_{ik} may take on values between zero and unity. Equation [36] satisfies the condition: $C_{nk} = 1$, which establishes that m_k is made up of the contributions of all sizes in the feed. Despite this condition, from a numerical standpoint there may be a number of p values for which: $m_{pk} = 0$; *i.e.*, not all the sizes in the feed contribute to size x_k in the population of particles. During the calculations, it was found that C_{ik} typically increased from zero to unity within a limited range of sizes in the feed. Therefore, the origin of any size x_k in the population of particles can be determined by plotting the cumulative contribution coefficient C_{ik} *vs* x_{i0} and finding the size interval in the feed in which C_{ik} increases from zero to unity.

The extension of the above procedure to all sizes x_k in the population of particles is shown in Figure 8, in which C_{ik} is plotted as a function of x_{i0} and x_{ik}. The values of C_{ik} are indicated by the scale on the right. As an example, an analysis is made for the receptacle

sample in run 17 of Table I. In Figure 8, the black, dashed diagonal joining the two opposite corners of the plot indicate the locations along which: $x_k = x_{i0}$. The use of the dashed diagonal will be evident in the following discussion.

To determine the sizes in the feed x_{i0} that contribute to a specific size in the receptacle x_k, draw a horizontal line at the given value of x_k. As an example, the case: $x_k = 25$ μm is shown. Next, beginning at the vertical axis on the left, move gradually to the right until the value of C_{ik} becomes greater than zero. In the example shown, this corresponds to: $x_{i0} = 27$ μm, which is signaled by the white dot next to the first arrow. As the horizontal trajectory is continued, it is found that C_{ik} becomes unity for: $x_{i0} = 210$ μm. Because both locations are below the dashed diagonal, it is concluded

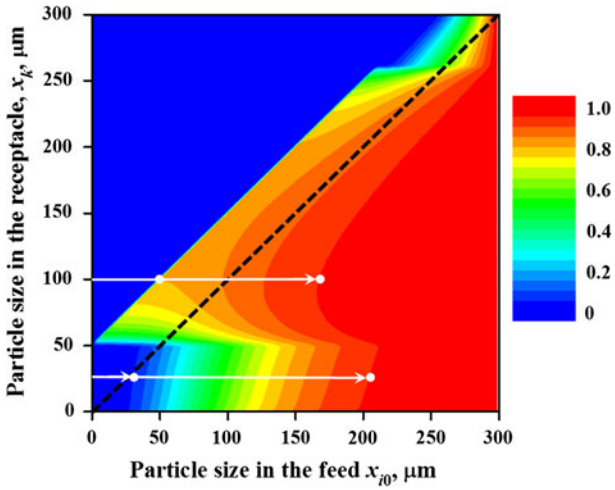

Fig. 8—Plot of the cumulative contribution coefficient C_{ik} computed from Eq. [36] in the receptacle of the laboratory furnace for run 17 in Table I. Values of C_{ik} are represented by the scale on the right. See the text for description.

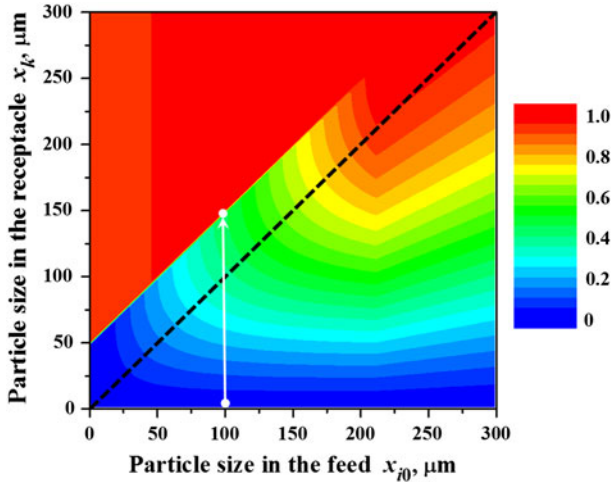

Fig. 9—Plot of the cumulative distribution coefficient D_{ik} computed from Eq. [37] in the receptacle of the laboratory furnace for run 17 in Table I. Values of D_{ik} are represented by the scale on the right. See the text for description.

that particles in the receptacle with size $x_k = 25$ μm resulted entirely from the fragmentation of sizes 27 to 210 μm in the feed.

A similar analysis can be made for other sizes x_k in the population of particles. Overall, the dashed diagonal in Figure 8 is a reference to indicate whether a specific size x_k in the population of particles originates from the expansion or fragmentation of a given size x_{i0} in the feed. In general, if at a given location: (x_{i0}, x_k) it is complied that: $C_{ik} > 0$, then x_k originated from the fragmentation of x_{i0} if (x_{i0}, x_k) is below the dashed diagonal. Similarly, x_k originated from the expansion of x_{i0} if (x_{i0}, x_k) is above the dashed diagonal. It is noted that some particles in the population may originate from both expansion and fragmentation of different sizes in the feed. An example of this situation is: $x_k = 100$ μm (also shown in Figure 8), which originated from sizes: 47 to 170 μm in the feed.

Based on the previous discussion, a complementary quantity was defined to track the destination of initial sizes in the feed in the particle population. Let m_{iq} be the mass of the initial size x_{i0} which ended up in size x_q in the population of particles at time t, where $0 < x_q < x_k$, and let m_{i0} be the mass of all the particles with initial size x_{i0} that entered the reactor. The cumulative distribution of size x_{i0} into all sizes in the population within the range: $0 < x_q \leq x_k$ is defined by

$$D_{ik} = \sum_{q=1}^{k} \frac{m_{iq}}{m_{i0}} \quad i = 1, n \;\; k = 1, \tilde{n} \qquad [37]$$

Symbol D_{ik} is referred to in this paper as the cumulative distribution coefficient of size x_{i0} into sizes up to x_k in the population of particles. Unlike the definition of C_{ik} given by Eq. [36], the values of D_{ik} may vary between zero and a positive value which is less than or equal to unity, *i.e.*, $0 \leq D_{ik} \leq 1$. This is because the mass of the individual particles in the feed m_{i0} is not conserved upon oxidation. According to the stoichiometry of Reaction

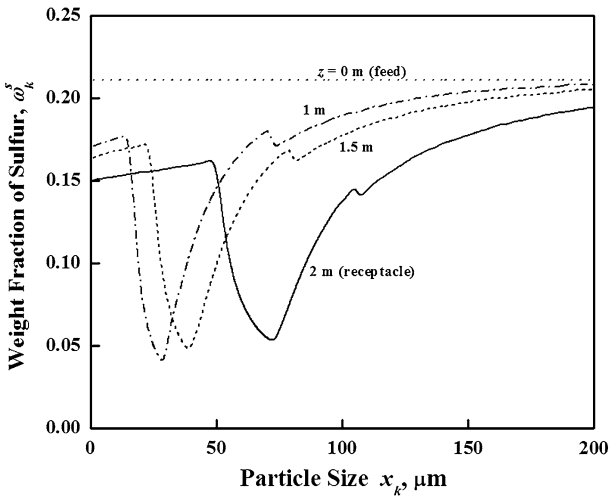

Fig. 10—Predicted evolution of sulfur content in the population of particles along the laboratory flash converting reactor for run 17 in Table I.

[B1] shown in Appendix, a single particle made up of copper matte ($Cu_2S \cdot yFeS_x$), loses 10 pct of its initial weight upon complete oxidation to Cu_2O and Fe_3O_4. Because the volatilization of the copper species and the presence of inerts in the particles were neglected, any weight change experienced by individual particles prior to fragmentation may be attributed to Reaction [B1]. Therefore, a limiting case is: $D_{i\tilde{n}} = 0.9$, which indicates that Reaction [B1] went to completion in all the particles with initial size x_{i0}. Because fragmentation was assumed to interrupt the oxidation reaction, it is concluded that such particles were completely oxidized in the reaction chamber before they started fragmentation. The other limiting case is: $D_{i\tilde{n}} = 1$, which implies that all the particles with initial size x_{i0} remained unreacted throughout the reaction chamber. This may be the case of large particles in the feed that did not reach their ignition temperature during flight. According to the present formulation, such particles may still have expanded and further fragmented. From the above considerations, the values of $D_{i\tilde{n}}$ are restricted to be within the range: $0.9 \leq D_{i\tilde{n}} \leq 1$.

Similar to the previous discussion on C_{ik}, there may be a number of q values in Eq. [37] for which: $m_{iq} = 0$, *i.e.*, particles with initial size in the feed x_{i0} do not distribute into all sizes in the population. Figure 9 shows the corresponding values of D_{ik} in the receptacle of the laboratory furnace for run 17 in Table I, in which the basic features of Figure 8 also apply.

To determine the sizes in the receptacle x_k to which a specific size in the feed x_{i0} distributes, draw a vertical line at the given value of x_{i0} and move upwards along that trajectory to identify the size range in the population of particles in which D_{ik} increases from zero to its maximum value. As an example, the case: $x_{i0} = 100$ μm is shown. From the above procedure, it is found that particles with initial size $x_{i0} = 100$ μm distributed to sizes: 1 to 150 μm in the receptacle. In this case: $D_{i\tilde{n}} = 0.977$, which indicates that particles with initial size $x_{i0} = 100$ μm were partially oxidized when they started fragmentation.

In Figure 9, the vertical trajectory along which D_{ik} increases from zero to its maximum value, crosses the dashed diagonal which represents the condition: $x_k = x_{i0}$. It is concluded that a portion of the particles with initial size: $x_{i0} = 100$ μm expanded and reached the receptacle with size 150 μm, whereas another portion expanded and further fragmented during flight to produce daughter particles in the range of 1 to 149 μm. In this analysis, it is noted that the initial size $x_{i0} = 100$ μm can distribute into sizes 100 to 149 μm only as a result of fragmentation. This is because all the particles in the feed were assumed to expand at a constant rate. Therefore, those particles with initial size x_{i0} that reached the receptacle without fragmenting have identical final size. This final size is the largest size into which x_{i0} distributed (150 μm), and is obtained from Eq. [1] by setting: $t = t_R$.

A new feature of the present model is its capability to track the chemical composition of the particle cloud as it travels through the reaction chamber. As an example, Figure 10 shows the evolution of the sulfur content as a function of particle size in the population for run 17 in Table I. The values shown in Figure 10 were computed from Eq. [27] at different locations along the reactor. Because all the particles in the feed entered the reactor with uniform composition, the plot at $z = 0$ m is a straight line parallel to the horizontal axis. It is of interest to note a minimum in sulfur content which moves toward larger sizes in the population as the particle cloud travels through the reaction chamber. Therefore, the size in which most oxidized particles can be found is dependent upon the time spent by the cloud in the reaction chamber. This trend occurs simultaneously with a decrease in sulfur content in dust particles (<20 μm) along the reactor.

These observations can be explained in terms of both expansion and fragmentation phenomena. Dust particles are made up of fragments of fully and partially oxidized particles. As the particle cloud travels through the reaction chamber, more particles fragment which contribute to dust. Because the fragments being produced farther down the reactor originate from more oxidized particles, those fragments decrease the sulfur content of dust particles along the reactor. Similarly, the minimum in sulfur content represents the size in the population which is continuously reaching the highest oxidation during expansion. Similar analyses can be made for other chemical elements in the particles such as copper, iron, and oxygen. However, such results are not shown here because they are mirror images of Figure 10. This is because copper, iron, sulfur, and oxygen contents in the particles are related to each other through the stoichiometry of the oxidation reaction described in Appendix.

Figures 7 to 10 show the potential of the present formulation as a useful tool for the analysis of a flash converting reactor. In a more general context, the model can be readily extended to other processes in which the main hypotheses stated in this work are valid, provided the appropriate kinetic model and the values of the model parameters are established accordingly. This includes but is not restricted to flash smelting of copper, nickel, and zinc concentrates.

IV. CONCLUDING REMARKS

A CFM for the oxidation of a cloud of sulfide particles in a flash reactor was developed. The model couples a population balance approach with the kinetic model of individual particles to compute the particle size distribution and chemical composition of the particle cloud as it travels through the reaction chamber.

The model showed good agreement with the experimental data collected in a laboratory flash converting reactor in terms of particle size distribution, amount of dust, and sulfur remaining in the population of particles. The cumulative contribution and distribution coefficients were introduced to analyze the coupled effects of reaction kinetics and size transformations of individual particles on the particle cloud characteristics. Because of its modular nature, the present formulation can readily be extended to similar systems such as flash smelting of copper, nickel, and zinc concentrates.

ACKNOWLEDGMENTS

Financial support for this investigation was provided by CONACyT (National Council of Science and Technology, Mexico) under project: CB-2008-104474-Y. Authors VRPS and CADR acknowledge CONACyT for providing the scholarship grants to conduct their graduate studies during this work.

APPENDIX A: COMPUTATION OF f_{if}

The symbol f_{if} represents the fraction of the initial size in the feed x_{i0} that has fragmented upon reaching the exit of the reactor. In the general case, f_{if} was assumed to vary linearly with x_{i0} within a size interval $[x_{\beta 0}, x_{\sigma 0}]$ which lies within the whole range of particle size $[x_{20}, x_{n0}]$. An example is shown in Figure A1, in which the values of f_{if} are represented by the solid line.

For numerical purposes, the smallest size in the feed x_{10} was assumed not to fragment. The location of the interval limits: $x_{\beta 0}$ and $x_{\sigma 0}$ may be computed by specifying the parameters f_{2f} and f_{nf} which are the extrapolated values of the straight solid line to sizes x_{20} and x_{n0}, respectively. The slope of the straight line is defined as p and is computed from

$$p = \frac{f_{nf} - f_{2f}}{x_{n0} - x_{20}} \qquad [A1]$$

Depending on the values of p, f_{2f} and f_{nf}, three cases are considered. The first case is shown in Figure A1, in which: $f_{2f} < 0$, $f_{nf} > 1$, and $p > 0$. The mathematical expression to compute f_{if} in this case is thus

$$f_{if} = \begin{cases} 0 & x_{20} \le x_{i0} < x_{\beta 0} \\ p(x_{i0} - x_{\beta 0}) & x_{\beta 0} \le x_{i0} < x_{\sigma 0} \\ 1 & x_{\sigma 0} \le x_{i0} \le x_{n0} \end{cases} \qquad [A2]$$

where: $x_{\beta 0} = -f_{2f}/p$, and $x_{\sigma 0} = (1 - f_{2f})/p$. The second case (not shown) occurs when f_{if} decreases with x_{i0} within the size interval $[x_{\beta 0}, x_{\sigma 0}]$. In this case $f_{2f} > 1$, $f_{nf} < 0$, and $p < 0$. The corresponding expression for f_{if} is

$$f_{if} = \begin{cases} 1 & x_{20} \le x_{i0} < x_{\beta 0} \\ 1 + p(x_{i0} - x_{\beta 0}) & x_{\beta 0} \le x_{i0} < x_{\sigma 0} \\ 0 & x_{\sigma 0} \le x_{i0} \le x_{n0} \end{cases} \qquad [A3]$$

where $x_{\beta 0} = (1 - f_{2f})/p$ and $x_{\sigma 0} = -f_{2f}/p$. Finally, the third case (not shown) occurs when $0 \le f_{2f} \le 1$ and $0 \le f_{nf} \le 1$, *i.e.*, the straight line spans over the entire size interval: $[x_{20}, x_{n0}]$. For this situation: $x_{\beta 0} = x_{20}$, $x_{\sigma 0} = x_{n0}$, and

$$f_{if} = f_{2f} + p(x_{i0} - x_{20}) \qquad [A4]$$

Depending on the pre-specified values of parameters f_{2f} and f_{nf}, the present formulation is thus capable of describing a variety of situations regarding particle fragmentation. It is noted that Eq. [A4] was the first approximation developed by the authors in the previous model.[17]

APPENDIX B: KINETIC MODEL FOR THE OXIDATION OF COPPER MATTE PARTICLES

The kinetic model is an adaptation of the model reported by Pérez-Tello *et al.*[19] for the oxidation of constant-size matte particles. In this study, particle oxidation was represented by the single chemical reaction

$$Cu_2S \cdot y FeS_{x\,(s)} + \left[\frac{3}{2} + y\left(x + \frac{2}{3}\right)\right] O_{2\,(g)} \rightarrow Cu_2O_{(s)} + \frac{y}{3} Fe_3O_{4\,(s)} + (1 + xy) SO_{2\,(g)} \qquad [B1]$$

Before particle melts, oxidation was assumed to occur at a sharp interface between the unreacted matte core and the product oxide layer according to a shrinking-core scheme. At this stage, both mass transfer and diffusion of gaseous oxygen through the porous oxide layer were assumed to control the rate of oxygen consumption. Upon solving the continuity equation for the oxygen within the porous oxide layer, the following expression for the rate of oxygen consumption at the matte-product interface is obtained

$$R_A = \frac{A_c r_p^2 (C_{Ab} - C_{Aeq})}{r_c^2 \left[\frac{1}{k_m} + \frac{r_p}{r_c}\frac{(r_p - r_c)}{D_{Aeff}}\right]} \qquad [B2]$$

in which C_{Aeq} was set to zero because the reaction may be assumed to be irreversible. Because r_p, r_c, k_m and D_{Aeff} on the right-hand side of Eq. [B2] are time-dependent, so is the rate of oxygen consumption, R_A. The particle radius r_p varies with time according to Eq. [1], in which $x_i = 2r_p$ and: $x_{io} = 2r_i$. The mass transfer coefficient k_m was obtained from the following expression

$$Sh = 2 + 0.6 Re_p^{1/2} Sc^{1/3} \qquad [B3]$$

where $Sh = 2r_p k_m / D_{AB}$ is the particle Sherwood number, $Re_p = 2r_p v_g \rho_g / \mu_g$ is the particle Reynolds number,

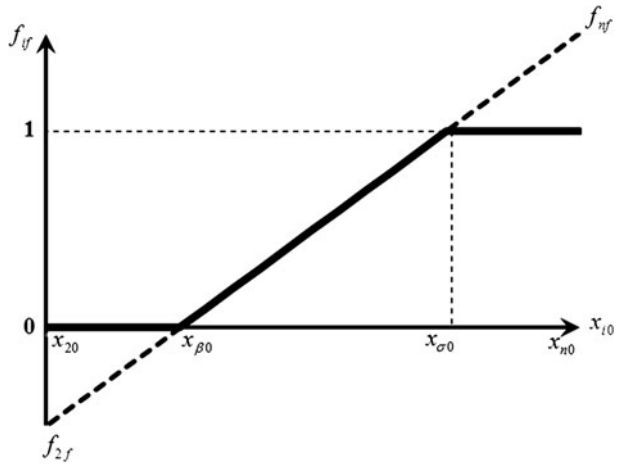

Fig. A1—Dependency of parameter f_{if} with the initial particle size x_{i0}.

and $Sc = \mu_g/(\rho_g D_{AB})$ is the gas-phase Schmidt number. In these expressions, all the gas properties were computed at the gas temperature T_g. The gas-phase oxygen diffusivity D_{AB} was computed from the Chapman–Enskog Equation[24] by considering the gas phase as a binary mixture of oxygen and nitrogen. The effective diffusivity of oxygen within the porous oxides D_{Aeff} was computed at the particle temperature T_p from the following expression[25]

$$D_{Aeff} = D_{AB}\psi/\tau \qquad [B4]$$

where ψ and τ are the porosity and tortuosity of the oxide layer, respectively. Because the particle was assumed to expand as soon as it enters the reaction chamber, the particle shell porosity ψ increases as the reaction proceeds. On the other hand, the tortuosity of the oxide layer τ was assumed to be constant along the particle trajectory. This property was used as a parameter to fit the model predictions to the experimental values of particle composition. Their values are shown in Table I.

Based on the stoichiometry of Reaction [B1], the rate of shrinking of the matte core is given by:

$$\frac{dr_c}{dt} = -\frac{bR_A}{\hat{\rho}_B A_c} \qquad [B5]$$

This expression was solved numerically to compute the matte core radius r_c as a function of time t. Once r_c is known, the amount of unreacted matte present in the particle was computed from the matte molar density $\hat{\rho}_B$ and the volume of the unreacted core, $(4/3)\pi r_c^3$. The amount of oxide species was thus computed from the stoichiometry of Reaction [B1]. Finally, the porosity of the oxide layer was obtained from the following expression

$$\psi = 1 - \frac{n_{Cu_2O}/\hat{\rho}_{Cu_2O} - n_{Fe_3O_4}/\hat{\rho}_{Fe_3O_4}}{4/3\pi(r_p^3 - r_c^3)} \qquad [B6]$$

The above shrinking-core model equations were assumed to be valid as long as the oxide layer in the particle remains solid. When the oxide layer completely melts, Reaction [B1] was assumed to be controlled by mass transfer of oxygen from the bulk gas to the surface of the reacting droplet. Under such conditions, the rate of oxygen consumption was computed from the following expression

$$R_A = A_p k_m (C_{Ab} - C_{Aeq}) f_s \qquad [B7]$$

where f_s is the fraction of the droplet surface occupied by the sulfides. This quantity was approximated by the volume fraction of the molten matte in the reacting droplet.

The numerical solution of Eqs. [B2] through [B6] provides the chemical composition of the individual particle and the particle mass, m_p. The particle temperature T_p was computed simultaneously from the particle energy balance

$$\frac{d(m_p h_p)}{dt} = A_p \varepsilon \sigma (T_w^4 - T_p^4) + hA_p(T_g - T_p) + (-\Delta H_R)R_A \qquad [B8]$$

Table B1. Values of the Parameters for the Kinetic Model

Parameter	Value
System pressure, P	87.1 kPa
Particle initial temperature, T_0	25 °C (298 K)
Temperature of incipient reaction, T_r	527 °C (800 K)
Melting point of unreacted core, T_{mc}	882 °C (1155 K)
Melting point of oxide layer, T_{mo}	1200 °C (1473 K)
Furnace wall/gas temperature, $T_g = T_w$	1077 °C (1350 K)
Molar density of matte, $\hat{\rho}_B$	31.6 kmol/m^3
Molar density of Cu_2O, $\hat{\rho}_{Cu_2O}$	37.7 kmol/m^3
Molar density of Fe_3O_4, $\hat{\rho}_{Fe_3O_4}$	22.4 kmol/m^3
Particle emissivity, ε	0.85
Heat of reaction, $(-\Delta H_R)$	$400 + 600y$ kJ/mol of matte
FeS_x to Cu_2S molar ratio, y	0.14
S to Fe atomic ratio, x	0.93
Particle residence time, t_R	0.9 s

where all the symbols are defined in the Nomenclature. Equation [B8] establishes that the accumulation of thermal energy within the particle is due to the exchange of heat between the particle and the furnace walls by radiation, the particle and gas by convection, and the generation of heat by the oxidation reaction. For simplicity, it was set: $T_w = T_g$ = constant, *i.e.*, suspension-smelting conditions were assumed. Because the particle mass m_p was computed from Eqs. [B2] through [B7], the numerical solution of Eq. [B8] provides the values of the specific enthalpy h_p along the particle trajectory. Once h_p is known, the particle temperature can be obtained by an iterative procedure involving the particle composition and the enthalpies of the individual species making up the particle. Details of the numerical algorithm are described elsewhere.[19] Along the particle trajectory, two phase changes may occur; first, the melting of the unreacted core at temperature T_{mc}; and second, the melting of the oxide layer at temperature T_{mo}.

Equations [B5] and [B8] were numerically solved by means of the Euler method.[22] Because Eq. [B8] shows a high degree of stiffness, the time discretization Δt was kept to a small value to maintain numerical stability. In this study, it was set at $\Delta t = 10^{-5}$ s. Table B1 shows the values of the parameters used to solve the kinetic model. With these specifications, the particle database $\Phi_i = \Phi_i(x_{i0}, t)$ was constructed and stored on disk prior to the fragmentation calculations. To keep the database within a manageable size, the data were stored every 1000 time steps.

NOMENCLATURE

A_c	Surface area of unreacted core (m^2)
A_p	Surface area of particle (m^2)
a, a_1, a_2	Parameters in Eqs. [32] and [33] (μm^{-1})
b	Stoichiometric coefficient = [3/2 + y(x + 2/3)]$^{-1}$
b, b_1, b_2	Parameters in Eqs. [32] and [33] (varies)
c, c_1, c_2	Parameters in Eqs. [32] and [33] (varies)

C_{Ab}	Oxygen concentration in the bulk gas (mol m^{-3})
C_{Aeq}	Equilibrium oxygen concentration (mol m^{-3})
C_{ik}	Cumulative contribution coefficient of particles up to size x_{i0} in the feed to particles with size x_k in the population (1)
C_3	Particle shape factor (1)
D_{ik}	Cumulative distribution coefficient of particles with size x_{i0} into sizes up to x_k in the population (1)
D_{Aeff}	Oxygen effective diffusivity in the oxide crust (m^2 s^{-1})
D_{AB}	Oxygen molecular diffusivity in the bulk gas (m^2 s^{-1})
DF	Degrees of freedom of Eq. [22] (1)
DG	Dust generation defined by Eq. [35] (1)
$F_{dust,f}$, $F_{dust,r}$	Fraction of dust in the feed and receptacle, respectively (1)
f_i	Fraction of the initial size in the feed x_{i0} that fragmented at time t
f_{if}	Fraction of the initial size in the feed x_{i0} that fragmented upon reaching the receptacle (1)
f_{2f}, f_{nf}	Fractions of the second smallest and the largest particles in the feed that fragmented upon reaching the receptacle, respectively (1)
f_s	Fraction of the droplet surface occupied by the sulfides (1)
$f_3(x_{i0})$	Density function of size x_{i0} in the feed (μm^{-1})
$f_3(x_k)$	Density function of size x_k in the population at time t (μm^{-1})
g	Particle expansion rate (μm s^{-1})
$g_3(x)$	Experimental density function in the receptacle of the laboratory furnace (μm^{-1})
$\overline{g_3(x)}$	Mean experimental density function in the receptacle of the laboratory furnace (μm^{-1})
h	Heat transfer coefficient (W K^{-1} m^{-2})
h_p	Particle specific enthalpy (J kg^{-1})
$(-\Delta H_R)$	Reaction enthalpy (J mol^{-1})
k_i	Proportionality constant in Eq. [9] (1)
k_m	Mass transfer coefficient (m s^{-1})
L	Reactor length (m)
m_{iq}	Mass of the initial size x_{i0} that ended up in size x_q in the population of particles at time t, where $0 < x_q < x_k$ (kg)
m_{i0}	Mass of particles with initial size x_{i0} in the feed (kg)
$m_{i\delta k}$	Mass of all daughter particles with size x_k that were produced from the initial size x_{i0} in the feed upon expanding to size x_δ prior to fragmentation (kg)
m_f	Total mass of particles that entered the reactor (kg)
m_{lk}	Mass of particles with size x_k that resulted from the expansion of all the particles with initial size x_{l0}, where $x_{l0} < x_k$ at time t (kg)
m_k	Total mass of particles with size x_k in the population at time t (kg)
m_k^q	Mass of species q in all the particles with size x_k in the population (kg)
m_k^S	Mass of sulfur in all the particles of size x_k in the particle population (kg)
$m_{k,0}^S$	Total mass of sulfur in all the particles of size x_k in the feed (kg)
m_{pk}	Mass of size x_k in the population of particles at time t that originated from the initial size in the feed x_{p0}, where $0 < x_{p0} < x_{i0}$ (kg)
m_r	Mass of particle population in the receptacle (kg)
$m_{\delta k}$	Mass of all daughter particles with size x_k that were produced from all initial sizes x_{i0} upon expanding to size x_δ prior to fragmentation (kg)
n	Number of sizes in the feed (1)
$\tilde{n}$	Number of sizes in the population at time t (1)
n_i	Number of particles with initial size x_{i0} in the feed that entered the reactor (1)
$m_{i\delta}^0$	Number of daughter particles produced by a single particle with initial size x_{i0} that expanded to size x_δ prior to fragmentation (1)
$n_{i\delta k}$	Number of particles with size x_k that were produced by all the particles with initial size x_{i0} that expanded to size x_δ prior to fragmentation (1)
$n_{i\delta k}^0$	Number of particles with size x_k that were produced by a single particle with initial size x_{i0} that expanded to size x_δ prior to fragmentation (1)
n_l	Number of particles that reached size x_k as a result of the expansion of smaller particles with size x_{i0} in the feed (1)
P	System pressure (kPa)
r^2	Correlation coefficient (1)
R_A	Rate of oxygen consumption in the particle (mol s^{-1})
r_c	Radius of the unreacted core in the particle (μm)
r_p	Particle radius (μm)
Re_p	Reynolds Number $= \frac{2r_p\langle v_g\rangle\rho_g}{\mu_g}$ (1)
Sc	Schmidt number $= \frac{\mu_g}{\rho_g D_{AB}}$ (1)
Sh	Sherwood number $= 2r_p k_m / D_{AB}$ (1)
$\langle S_{rem}\rangle$	Fraction of the initial sulfur remaining in the particle population (1)
t	Time (s)
t_{ic}	Time spent by a single particle with size x_{i0} to achieve its critical size x_{ic} (s)
t_R	Particle residence time in the reaction chamber (s)

T_g	Gas temperature (K)
T_{mc}	Melting temperature of the sulfides (K)
T_{mo}	Melting temperature of the oxides (K)
T_p	Particle temperature (K)
T_r	Incipient reaction temperature (K)
T_w	Furnace wall temperature (K)
T_0	Particle initial temperature (K)
v	Particle velocity (m s^{-1})
v_g	Gas velocity (m s^{-1})
x	S to Fe atomic ratio (1)
x_i	Size of the ith size in the feed at time t (μm)
x_{ic}	Critical size at which the initial size x_{i0} starts to fragment (μm)
x_{i0}	Size of the ith particle size fraction in the feed (μm)
x_k	Particle size in the population of particles at time t (μm)
x_{l0}	Initial size of particles that reached the size x_k after they expanded (μm)
x_{10}, x_{20}, x_{n0}	Smallest, second smallest, and largest particle size in the feed, respectively (μm)
$x_{i\delta}$	Size achieved by the initial size x_{i0} upon expansion prior to immediate fragmentation (μm)
y	Moles of FeS_x per mole of Cu_2S in matte particle (1)
z	Axial distance from the burner tip (m)

GREEK SYMBOLS

Δt	Time increment (s)
Δx_{i0}, Δx_k	Size discretization (μm)
γ	Fragmentation distribution parameter (1)
ε	Particle emissivity (1)
ψ	Porosity of the oxide layer (1)
$\lambda_{i\delta k}$	Number fraction of daughter particles with size x_k originated by a single particle with size x_{i0} in the feed that reached size x_δ prior to fragmentation (1)
μ_g	Gas viscosity (kg m^{-1} s^{-1})
$\hat{\rho}_B$	Molar density of matte (mol m^{-3})
ρ_g	Gas density (kg m^{-3})
$\rho_{i\delta}$	Apparent density of particles with size x_δ originating from the expansion of particles with size x_{i0} in the feed (kg m^{-3})
$\rho_{i\delta k}$	Apparent density of daughter particles with size x_k originating from particles with size x_{i0} in the feed that reached size x_δ prior to fragmentation (kg m^{-3})
ρ_{lk}	Apparent density of particles with size x_k originating from the expansion of particles with size x_{l0} in the feed (kg m^{-3})
ρ_0	Density of particles in the feed (kg m^{-3})
σ	Stefan-Boltzmann constant (W m^{-2} K^{-4})
τ	Tortuosity of the oxide layer (1)
Φ_i	Generalized property of a single particle with initial size x_{i0} during oxidation and expansion at time t (varies)
$\omega^q_{i\delta}$	Mass fraction of the q-species in particles with size x_δ originating from the expansion of particles with size x_{i0} in the feed (1)
$\omega^q_{i\delta k}$	Mass fraction of the q-species in daughter particles with size x_k originating from particles with size x_{i0} in the feed that reached size x_δ prior to fragmentation (1)
ω^q_{lk}	Mass fraction of the q-species in particles with initial size x_{l0} that reached size x_k upon expansion (1)
ω^q_k	Mass fraction of the q-species in all the particles with size x_k in the particle population (1)
ω^S_k	Sulfur mass fraction in all the particles with size x_k in the particle population (1)
$\omega^S_{k,0}$	Sulfur mass fraction in all the particles with size x_k in the particle population in the feed (1)
$\langle\omega^q\rangle$	Mass fraction of the q-species in the particle population (1)

REFERENCES

1. F.R. Jorgensen and E.R. Segnit: *Proc. Australas. Inst. Min. Metall.*, 1977, vol. 261, pp. 39–46.
2. F.R. Jorgensen: *Proc. Australas. Inst. Min. Metall.*, 1980, vol. 276, pp. 41–47.
3. F.R. Jorgensen: *Trans. Inst. Min. Metall. C*, 1981, vol. 90, pp. C10–C16.
4. F.R. Jorgensen: *Trans. Inst. Min. Metall. C*, 1981, vol. 90, pp. C1–C9.
5. F.R. Jorgensen: *Proc. Australas. Inst. Min. Metall.*, 1983, vol. 288, pp. 37–46.
6. Y.H. Kim and N.J. Themelis: *The Reinhardt Schuhmann International Symposium on Innovative Technology and Reactor Design in Extractive Metallurgy*, D.R. Gaskell, J.P. Hager, J.E. Hoffman, and P.J. Mackey, eds., TMS, Warrendale, PA, 1986, pp. 349–69.
7. N. Kemori, W.T. Denholm, and H. Kurokawa: *Metall. Trans. B*, 1989, vol. 20B, pp. 327–36.
8. A.T. Jokilaakso, R.O. Suominen, P.A. Taskinen, and K.R. Lilius: *Trans. Inst. Min. Metall. C*, 1991, vol. 100, pp. C79–C90.
9. A. Otero, J.K. Brimacombe, and G.G. Richards: *Copper 91-Cobre 91*, C. Díaz, C. Landolt, A. Luraschi, and C.J. Newman, eds., Pergamon, Ottawa, ON, 1991, pp. 459–73.
10. R.O. Suominen, A.T. Jokilaakso, P.A. Taskinen, and K.R. Lilius: *Scand. J. Metall.*, 1991, vol. 20 (4), pp. 245–50.
11. A. Warczok and T.A. Utigard: *EPD Congress 1992*, J.P. Hager, ed., The Minerals, Metals and Materials Society, Warrendale, PA, 1991, pp. 729–44.
12. H.Y. Sohn and P.C. Chaubal: *Metall. Trans. B*, 1993, vol. 24B, pp. 975–85.
13. R.O. Suominen, A.T. Jokilaakso, P.A. Taskinen, and K.R. Lilius: *Scand. J. Metall.*, 1994, vol. 23 (1), pp. 30–36.
14. A. Thomas, J.R. Grace, and I.V. Samarasekera: *Can. Metall. Q.*, 2000, vol. 39 (2), pp. 187–93.
15. F.R.A. Jorgensen and P.T.L. Koh: *JOM*, 2001, vol. 53 (5), pp. 16–20.
16. F.R.A. Jorgensen: *Sulfide Smelting 2002*, R.L. Stephens and H.Y. Sohn, eds., The Minerals, Metals & Materials Society, Seattle, Washington, 2002, pp. 49–60.
17. M. Perez-Tello, I. Madrid-Ortega, and H.Y. Sohn: *Min. Metall. Proc.*, 2008, vol. 25, pp. 53–60.
18. M. Perez-Tello, H.Y. Sohn, K. St Marie, and A. Jokilaakso: *Metall. Mater. Trans. B*, 2001, vol. 32B, pp. 847–68.

19. M. Perez-Tello, H.Y. Sohn, and P.J. Smith: *Metall. Mater. Trans. B*, 2001, vol. 32B, pp. 869–86.
20. R.P. King: *J. South African Inst. Min. Metall.*, 1973, vol. 73, p. 127.
21. M. Perez-Tello, J.A. Tirado-Ochoa, H.Y. Sohn, and V.M. Sánchez-Corrales: *JOM*, 2002, vol. 54 (10), pp. 27–30.
22. W.H. Press: *Fortran Numerical Recipes*, 2nd ed., Cambridge University Press, Cambridge, 1996.
23. A.A. Shook, G.G. Richards, and J.K. Brimacombe: *Metall. Mater. Trans. B*, 1995, vol. 26B, pp. 719–29.
24. R.B. Bird, W.E. Stewart, and E.N. Lightfoot: *Transport Phenomena*, Rev. 2nd ed., Wiley, New York, 2007.
25. A.L. Hines and R.N. Maddox: *Mass Transfer: Fundamentals and Applications*, Prentice-Hall, Englewood Cliffs, NJ, 1985.